NUCLEAR REACTIONS -- THEORY

THE DISAPPEARANCE OF FUSION-LIKE RESIDUES AND THE NUCLEAR EQUATION OF STATE

H.M. Xu, W.G. Lynch, P. Danielewicz and G.F. Bertsch

To investigate the dynamical limits to the formation of hot composite nuclei, heavy residue cross sections were calculated for $^{40}Ca + ^{40}Ca$ and $^{40}Ar + ^{27}Al$ collisions using the Boltzmann equation.[1] Qualitatively consistent with experimental observations,[2] the calculated heavy residue cross sections decrease rapidly to zero for E/A > 35-40 MeV. The decrease in cross section does not appear related to a bulk instability of nuclei at high temperature.[2,3]

The calculations were performed by solving numerically the Boltzmann equation that includes mean-field and Pauli blocking terms. The mean field potential consisting of the Coulomb potential and a nuclear potential with isoscaler and symmetry terms.[4] The isoscaler potential field U_o was approximated by

$$U_o(\rho) = -A\rho/\rho_o + B(\rho/\rho_o)^\gamma \quad \text{(MeV)}. \qquad (1)$$

Values for A, B, and γ, given in Table 1, were used in specific calculations to provide soft (K=200 MeV) or hard (K=375 MeV) equations of state. To ensure the conservation of total energy, the Lattice Hamiltonian method of Lenk and Pandharipande was used.[5] This method ensured energy conservation to better than 0.1 MeV per nucleon over a time period of about 300 fm/c.

To illustrate the features of these calculations we consider calculations for $^{40}Ca + ^{40}Ca$ system at E/A = 40 MeV. For this system, calculations were performed for $\sigma_{NN} = \frac{4\pi \cdot d\sigma(\Omega)}{d\Omega}_{nn} = 41$ mb and both soft and stiff equations of state. Figure 1 shows the masses (upper left panel) and the component of velocity parallel to the beam axis (lower left panel) of heavy residues produced in the calculations. Two residues with $30 \leq A \leq 40$ are produced at large impact parameters b > 3.3 fm for calculations with the stiff EOS (open points) and the soft EOS (open squares). A single heavy residue is observed at small impact parameters, $b \leq 3.3$ fm, in calculations with the stiff EOS (solid points). For small impact parameters with the soft EOS, however, the projectile and target simply pass through each other, with their velocities and masses reduced. (More complicated multi-fragment final states are suppressed by the ensemble averaging of the mean field potential.) The total orbital

Table 1: Mean Field Parametrizations

Set	Label	range	A(MeV)	B(MeV)	γ	K(ρ=ρ$_o$)(MeV)
1	soft	$0<\rho/\rho_o<\infty$	356	303	7/6	200
2	stiff	$0<\rho/\rho_o<\infty$	124	70.5	2	375
3	soft-stiff	$\rho/\rho_o<1.024$	356	303	7/6	
		$1.024<\rho/\rho_o$	124	70.5	2	
4	stiff-soft	$\rho/\rho_o<1.024$	124	70.5	2	
		$1.024<\rho/\rho_o$	356	303	7/6	

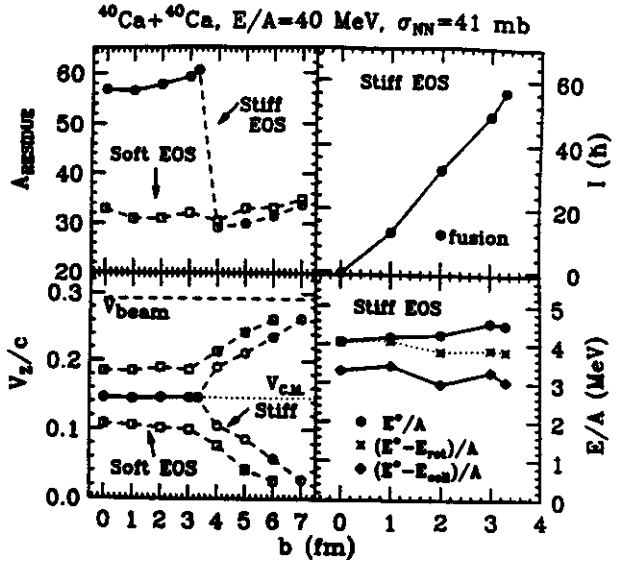

Fig. 1. Observables calculated for the ^{40}Ca+^{40}Ca system at E/A=40 MeV assuming σ_{NN}=41 mb. Upper left: Mean residue masses. Lower left: Component of the mean residue velocity parallel to the beam. Upper right: Mean residue angular momentum for the stiff EOS. Lower right: Mean residue total excitation energy/nucleon (solid points), after subtracting the rotational energy (crosses), and after subtracting the total collective energy (solid diamonds) for calculations with the stiff EOS. The lines are drawn to guide the eye.

angular momentum of the fusion-like residue produced in calculations with the stiff EOS (upper right panel) increases linearly with impact parameter to a value of about 60 ħ at b=3.3 fm, comparable to the maximum orbital angular momentum predicted by the liquid-drop model. This suggests that formation of a residue may be partially limited by angular momentum considerations.

The total excitation energy of the residues is shown at t = 120 fm/c by the solid points in the lower right hand panel in Fig. 1 for fusion-like residues produced in calculations with the stiff EOS. The total excitation energy increases slightly with impact parameter; this increase is partly due to the collective energy of rotation. The solid crosses depict the excitation energy after the rotational energy has been subtracted. To enable more accurate estimations of the thermal excitation of the residue, a collective velocity field was defined on the computational lattice,[6] and an integration was performed to obtain a total kinetic energy of collective motion. After subtracting the total collective energy, the intrinsic excitation energy, designated by the solid diamonds, decreases slightly with impact parameter. Thus in these dynamical calculations, the formation of heavy residues does not appear to be limited by the stability of the residual nucleus at high temperature. Indeed, in larger impact parameter collisions, where residue formation is tenuous, the intrinsic excitation energies are somewhat smaller.

The energy dependences of the incomplete fusion cross sections for calculations with soft and stiff equations of state are indicated respectively by the solid squares and solid points in the upper half of Fig. 2. Each symbol

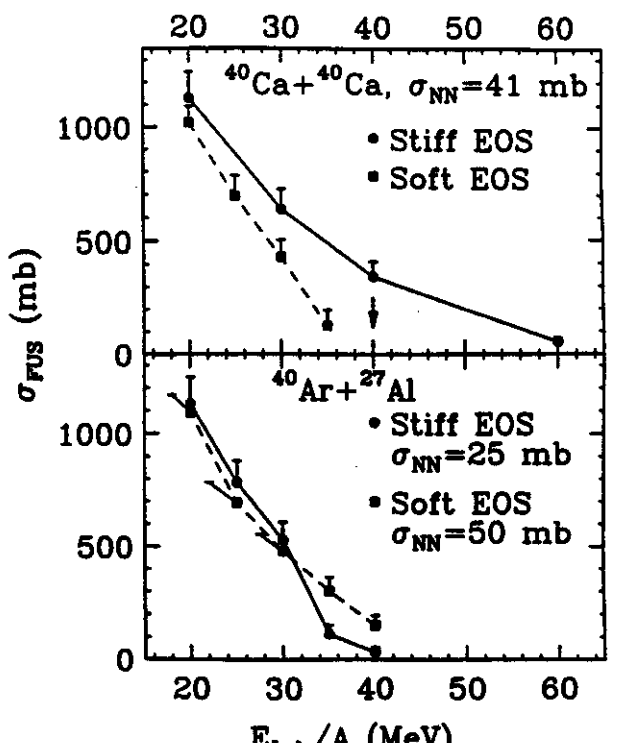

Fig. 2. Upper half: Residue cross sections for ^{40}Ca+^{40}Ca collisions. Lower half: Residue cross sections for ^{40}Ar+^{27}Al collisions. The solid points and solid squares describe calculations with the stiff and soft equations of state, respectively. The lines are drawn to guide the eye.

(square or point) is obtained from the largest calculated impact parameter which yielded massive fusion-like residues; the upper edge of each vertical bar corresponds to the smallest calculated impact parameter which yielded distinct projectile- and target-like residues. For a constant nucleon-nucleon cross section of 41 mb, the cross sections for fusion-like residues are significantly larger for calculations with the stiff EOS.

To explore separately the sensitivity of the calculations to the form of the EOS at high and low density, calculations were performed with the soft-stiff and stiff-soft equations of state, corresponding to mean field parameter sets 3 and 4 in Table 1, respectively. The mean potential field for the soft-stiff EOS is identical to the potential for the soft EOS at low density, $\rho < 1.024\rho_o$, and identical to the potential field for the stiff EOS at high density, $\rho > 1.024\rho_o$. For the stiff-soft EOS the matching point remains the same but the choices of mean field potential parametrizations at high and low density are reversed. In calculations with the $^{40}Ca+^{40}Ca$ system at E/A = 40 MeV, a heavy residue cross section of 330±30 mb was obtained with the stiff-soft EOS, equal to that for the stiff EOS. In contrast, the cross section for the soft-stiff EOS was only 120±20 mb, nearly a factor of three smaller. This indicates that the fusion cross sections are mainly sensitive to the EOS at low density.

A possible determination of the low-density EOS on the basis of the cross sections for residue formation is hindered by the fact that these cross sections are also sensitive to σ_{NN}. To illustrate the possible theoretical ambiguities, calculations were performed for the $^{40}Ar+^{27}Al$ system in which the value for σ_{NN} was adjusted separately for calculations with both stiff and soft equations of state to obtain residue cross sections of about 500 mb at E_{Lab}/A = 30 MeV. These choices, (1) σ_{NN} = 25 mb and a stiff EOS and (2) σ_{NN} = 50 mb and a soft EOS, provide essentially equal residue cross sections at E/A ≤ 30 MeV. The energy dependence of the residue cross sections predicted by both calculations is qualitatively consistent with experimental observations.[2] Differences between the two sets of calculations at $E_{Lab}/A > 30$ MeV may not be enough to discriminate between different equations of state.

Measurements of additional observables may help to reduce these ambiguities. For example, the top panel in Fig. 3 shows the corresponding

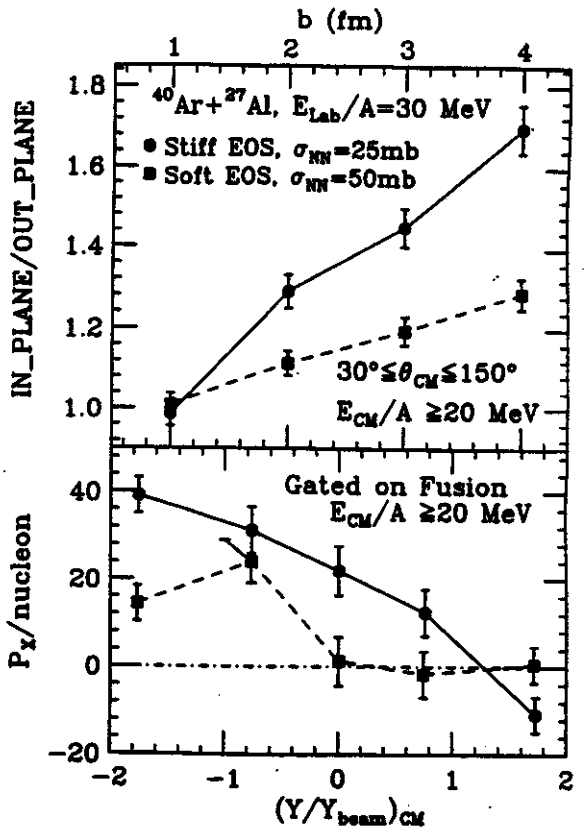

Fig. 3. In/out-of-plane ratios and mean transverse momenta for unbound nucleons with $E_{c.m.} \geq 20$ MeV from calculations for the $^{40}Ar+^{27}Al$ system at E/A = 30 MeV for σ_{NN}=25 mb, stiff EOS (solid points) and σ_{NN}=50 mb, soft EOS (solid squares). Upper half: Ratios of the nucleon yield in the reaction plane to the nucleon yield out of the reaction plane. Integrations have been performed over the polar angles $30° \leq \theta_{cm} \leq 150°$ and the azimuthal angles $60° < \phi < 120°$ and $240° < \phi < 300°$ for the out-of-plane yields and $-30° < \phi < 30°$ and $150° < \phi < 210°$ for the in-plane yields. Lower half: The component of the mean transverse momentum of unbound nucleons in the reaction plane as a function of rapidity. A weighted sum over impact parameters b≤4 fm has been performed. The lines are drawn to guide the eye.

predictions for the ratio of the yield of nucleons emitted in the reaction plane over the yield emitted out of the reaction plane for center of mass angles, $30° \leq \theta_{c.m.} \leq 150°$, and energies, $E_{cm} \geq 20$ MeV. Calculations with the soft EOS and σ_{NN}=50 mb are more isotropic. The greater isotropy of calculations with larger σ_{NN} is also manifested in the dependence of the mean transverse momentum of emitted nucleons upon rapidity, shown in the bottom panel of Fig. 3. Significantly transverse momenta are predicted at $Y < Y_{beam}$ for calculations with smaller values for σ_{NN}. Even larger anisotropies would be expected for deuterons, tritons or α particles within the coalescence approximation for cluster emission. Given advances in the treatment of cluster production, such large anisotropies in the emission of the heavier hydrogen and helium isotopes could provide significant constraints on σ_{NN} and consequently, on the EOS if anisotropy measurements are combined with heavy residue cross sections.

Some caution must be exercised when comparing these residue cross sections to experimental data. Since these excited residues will decay, all residue decay channels, including the binary emission of heavy fragments, must be experimentally measured and summed before comparisons to the calculated cross sections of Fig. 2 can be made.

In summary, calculations have been performed with the Boltzmann equation to assess the sensitivity of heavy residue cross sections to the EOS and the in-medium nucleon-nucleon cross section. For specific choices of σ_{NN} and the nuclear EOS, the calculated residue cross sections decrease and eventually vanish for incident energies above E/A ≥ 35 MeV, consistent with experimental observations. This decrease in cross section does not seem to be related to a bulk instability of nuclei at high temperature. The calculated residue cross sections are sensitive to both the nuclear EOS and the nucleon-nucleon cross section. This dual sensitivity constitutes an ambiguity which may be reduced or eliminated by measurements of observables like the in/out-of-plane ratio and the mean transverse momentum that are related to the isotropy of the emission patterns of coincident light particles.

References

1. G.F. Bertsch, H. Kruse and S. Das Gupta, Phys. Rev. C29(1984)673.
2. S. Leray, J. Phys. Colloq. 47 C4(1986)275.
3. S. Levit and P. Bonche, Nucl. Phys. A437,(1984)426.
4. M.B. Tsang, G.F. Bertsch, W.G. Lynch and Mitsuru Tohyama, Phys. Rev. C40(1989)1685.
5. R.J. Lenk and V.R. Panharipande, Phys. Rev. C39(1989)2242.
6. B. Remaud, C. Gregoire, F. Sebille and P. Schuck, Nucl. Phys. A488(1988)423c.

DISAPPEARANCE OF FLOW AND THE IN-MEDIUM NUCLEON-NUCLEON CROSS SECTION

W. Bauer, C.A. Ogilvie, D. Krofcheck, and G.D. Westfall

We measured the transverse collective momentum in heavy ion collisions of ^{40}Ar projectiles with ^{51}V targets in the beam energy range between 35 and 100 MeV/nucleon with the MSU 4π-array. We observed a minimum in the collective sidewards flow in central collisions at a beam energy of 82 ± 3 MeV/nucleon.[1,2] This was deduced from the data in Fig. 1 by taking the beam energy to be the ordinate of the minimum point of the fitted parabola.

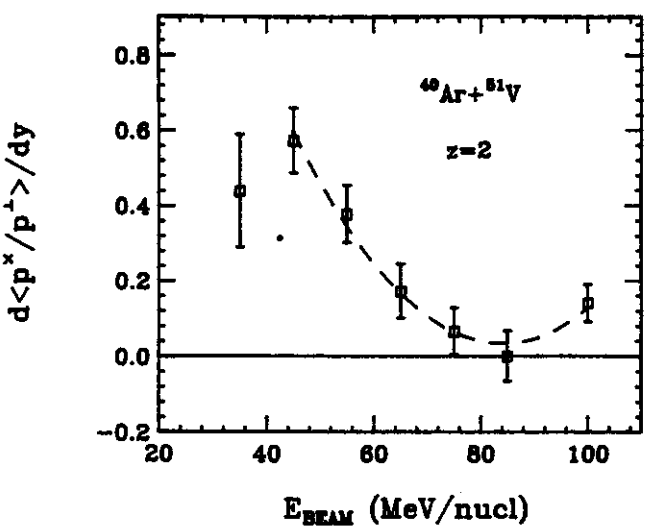

Fig. 1 The flow excitation function for Z=2 fragments from the Ar+V reaction.

The disappearance of flow is the result of a cancellation between the mean field attractive interaction, which results in a deflection of the fragments to predominantly negative scattering angles, and the repulsive pressure build up due to the compression of nuclear matter, which is known to deflect the fragments primarily to positive scattering angles. The main motivation for investigating the detailed excitation function is to try to understand the nuclear reaction mechanism in more detail and to narrow the window of possible values for the parameters of the nuclear equation of state.

To obtain qualitative measures for the sensitivity to the different degrees of freedom of nuclear matter, we performed detailed test calculations using the nuclear Boltzmann-Uehling-Uhlenbeck transport computer code as described in Ref. 3. In order to be able to obtain a realistic comparison between experimental data and numerical results, we subjected the theoretical output to the same acceptance filter that was imposed on the data by the detector cutoffs.

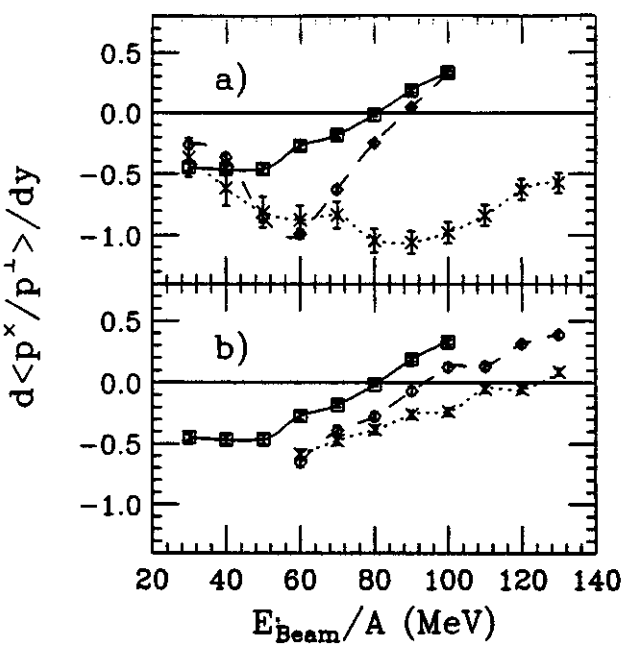

Fig. 2 Sensitivity of the point of vanishing nuclear collective flow to a) the stiffness of the nuclear equation of state and b) the in-medium nucleon nucleon cross section in a BUU simulation of the flow excitation function for the reaction Ar + V.

In Fig. 2, the main results of our theoretical study are summarized. In part a), we compare the theoretical results obtained from different nuclear compressibilities. The solid line and dashed line are obtained using the values of 200 MeV and 380 MeV for the nuclear compressibility. As can be seen, the point of

disappearing flow is only slightly different in the two cases (80 MeV/nucleon beam energy vs. 88). For comparison, the dotted line shows the results of a calculation in which we also used a soft equation of state (200 MeV compressibility), but solved only the Vlasov equation without nucleon-nucleon collisions. Obviously, the effect of avoiding two-body collisions is much larger, and the attractive flow still persists at beam energies of 140 MeV/nucleon and above.

In part b), we therefore study the dependence of the point of vanishing flow on the nucleon-nucleon in-medium cross section for a soft equation of state. The solid, dashed and dotted lines correspond to values of σ/σ_{free} = 1.0, 0.9 and 0.7, respectively. As can be seen from this figure, the disappearance point is very sensitive to the in-medium nucleon-nucleon cross section. Our results indicate that the in-medium nucleon nucleon cross section has roughly (within 10%) the same value as the free elementary cross section for this reaction.

References

1. C.A. Ogilive et al., submitted to Phys. Rev. C.
2. W. Bauer, Preprint MSUCL-699, submitted to Phys. Rev. C.
3. D. Krofcheck et al., submitted to Phys. Rev. C.

SINGLE-PHOTON DECAY OF THE Δ-RESONANCE IN HEAVY ION COLLISIONS

Wolfgang Bauer and George F. Bertsch

Recently, Prakash et al.[1] suggested that the decay $\Delta \rightarrow N + \gamma$ should result in a visible enhancement (factor 10) of the total photon production cross section for photon energies greater than 200 MeV in heavy ion collisions at beam energies as low as 44 MeV/nucleon. They arrived at their conclusion by examining photo-absorption cross sections of nuclei and using the principle of detailed balance.

Contrary to this prediction, an MSU group has not seen the expected change in shape of the photon spectrum due to the excitation of the Δ resonance in the reaction of $^{14}N + Zn$ at a beam energy per nucleon of 75 MeV.[2] We have therefore performed calculations to resolve this contradiction.[3]

For our investigation, we numerically solve the nuclear Boltzmann-Uehling-Uhlenbeck transport equation (BUU). In this model, the Δ-resonance is produced in nucleon-nucleon collisions with a mass distribution as parameterized by Kitazoe et al.[4] For the branching ratio to the process $\Delta \rightarrow N + \gamma$, we use the experimentally measured value of 0.6%.

We also calculate the photons produced via the decay of neutral pions, $\pi^0 \rightarrow 2\gamma$, and the direct Bremsstrahlung photons produced in individual neutron-proton collisions[5] to obtain information on which process dominates the photon spectrum at high energies.

In Fig. 1, the results of our calculations for the two beam energies 75 and 200 MeV/nucleon are summarized. The histograms represent the photon production cross section from the single-photon decay of the Δ-resonance, the dashed lines shows the contribution of the electromagnetic decay of the neutral pions, and the solid line is the Bremsstrahlung cross section. For the higher beam energy, we were not able to perform the Bremsstrahlung calculation reliably, and it is therefore omitted. However, it is experimentally known that at the higher energy the pion-decay contribution dominates the Bremsstrahlung

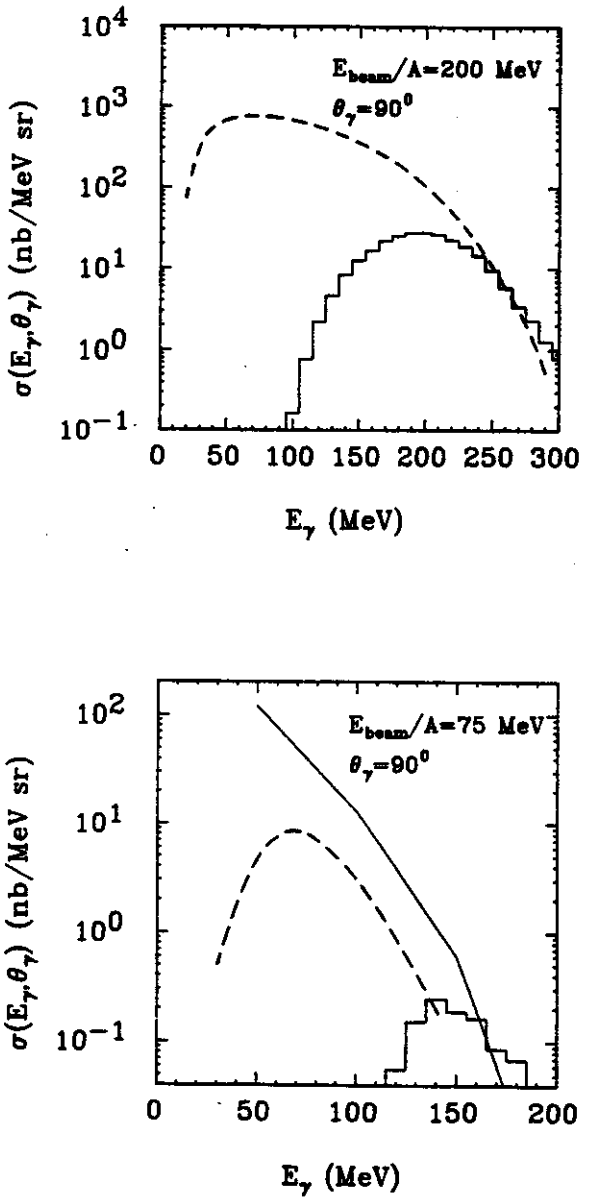

Fig. 1. Calculated contributions of the single-photon decay of the Δ-resonance (histogram), Bremsstrahlung (solid line), and neutral pion decay (dashed line) to the the total photon production cross section.

contribution to the photon production cross section.

One can see that at 75 MeV/nucleon the single-photon Δ-decay cross section is of the same order as the Bremsstrahlung cross section, and therefore no large enhancement due to this process should be observed. This is in accordance with experiment. However, at 200 MeV/nucleon, this process is comparable in cross section to the neutral pion decay process for photon energies greater than 200 MeV. By careful subtraction of the pion decay background, the single-photon decay of the Δ-resonance should then be observable and might yield insight into the propagation of exited nucleonic states through nuclear matter.

References

1. M. Prakash, P. Braun-Munzinger, J. Stachel, and N. Alamanos, Phys. Rev. C37,1959(1988).
2. J. Clayton and J. Stevenson, private commuication.
3. W. Bauer and G.F. Bertsch, Phys. Lett. 229B, 16(1989).
4. Y. Kitazoe, M. Sano, H. Toki, and S. Nagamiya, Phys. Lett. 166B,35(1986).
5. W. Bauer, G.F. Bertsch, W. Cassing, and U. Mosel, Phys. Rev. C34,2127(1986); W. Bauer, Phys. Rev. C40,715(1989).

CRITICAL PION OPACITY

Wolfgang Bauer

The classical phenomenon of critical opacity is an increased scattering of electromagnetic radiation near to the critical point of a substance.[1] Far away from T_c, there is no appreciable light scattering. As T_c is approached, however, the sample takes on a milky appearance. This is due to the scattering of light off the density fluctuations.

We expect nuclear matter to have a phase diagram similar to a Van der Waals gas, because the nuclear interaction exhibits short range repulsion and long range attraction. It should be stressed at this point that there is not firm experimental evidence for the existence of a second order phase transition and a corresponding critical point as of yet. However, it is hoped that with the new heavy ion accelerators and 4π detectors this interesting point of the nuclear phase diagram will be studied in detail. In a previous publication, we have pointed out methods to look for the critical point and to determine the critical exponents.[2]

Here we propose a new effect that should occur as we approach the critical point of nuclear matter from above, as a function of the order parameter. It is the decrease of transparency of nuclear matter near the critical point for pions traversing it, and we have therefore dubbed it "Critical Pion Opacity".

To see how this effect arises, we note that pion absorption is (at least) a two-nucleon process. The absorption of a pion on one nucleon is forbidden for simple kinematical reasons. The dominant channel for pion absorption is the so-called Delta process, in which a nucleon is excited to the isospin 3/2 Delta resonance state by the incoming pion. This Δ can then interact with a second nucleon via $\Delta + N \rightarrow N + N$ to complete the process of the pion absorption. This process has to take place at short interparticle distances between the two nucleons because of the short lifetime of the Δ. Thus the pion absorption cross section exhibits a dependence of $\sigma_{abs} \propto \rho^{\lambda}$, with $\lambda \geq 2$, and is therefore sensitive to the fluctuations in the density. If we could irradiate nuclear matter at its critical point with pions, we should see the effects of the density fluctuations in the pion absorption cross section.

One of the ways in which we believe we can experimentally reach the critical point of nuclear matter is in symmetric heavy ion collisions with beam energies around 100 MeV/nucleon. During the compression phase of this reaction, densities of 1.5 to 2 ρ_0 are reached and some pions are produced. The overall excitation function for these "subthreshold" pions is well understood in this beam energy domain.[3] Even though there is a large amount of absorption during this high density phase of the collision, some pions escape from this high density phase. To experience the effect of density fluctuations near the critical point, the pions have to stay in the baryon matter long enough for it to expand to the critical point.

We have estimated the maximum kinetic energy allowed for these pions. To do this, we used a simple hydrodynamical model and the nuclear equation of state of Ref. 4 for the expansion of the baryon matter. We find that the baryon system typically takes on the order 20-30 fm/c to reach the critical density, it it was initially compressed to twice nuclear matter density. This time scale corresponds to a kinetic energy of approximately 20 MeV in the center of mass system for a pion produced at t=0 in the center of the baryon matter.

We suggest the following way to measure the effect of critical pion opacity. As a function of beam energy, one should measure the total

pion cross section for pions with kinetic energy less than the above value in the center of mass system and divide it by the total cross section for pions with kinetic energy above this value. Our prediction is that one should observe a large decrease in this ratio as one passes the beam energy corresponding to the critical point from above.

References

1. H.E. Stanley, Introduction to Phase Transitions and Critical Phenomena, Oxford University Press (1971).
2. W. Bauer, Phys. Rev. C38,1297(1988).
3. W. Bauer, Phys. Rev. C40,715(1989).
4. J. Kapusta, Phys. Rev. C29,1735(1984).

MULTIPARTICLE INTERACTIONS IN HIGH-ENERGY COLLISIONS WITH NUCLEI

P. Danielewicz and Boyong Chen

High-energy collisions with nuclei are commonly treated as a superposition of elementary binary collisions of particles. Within such treatment, however, one cannot account for the phenomenon of backward particle production,[1] and findings from electron scattering.[2] There are also difficulties in explaining the subthreshold particle production[1]. We attempt to describe the experimental results in terms of multiparticle interactions[3].

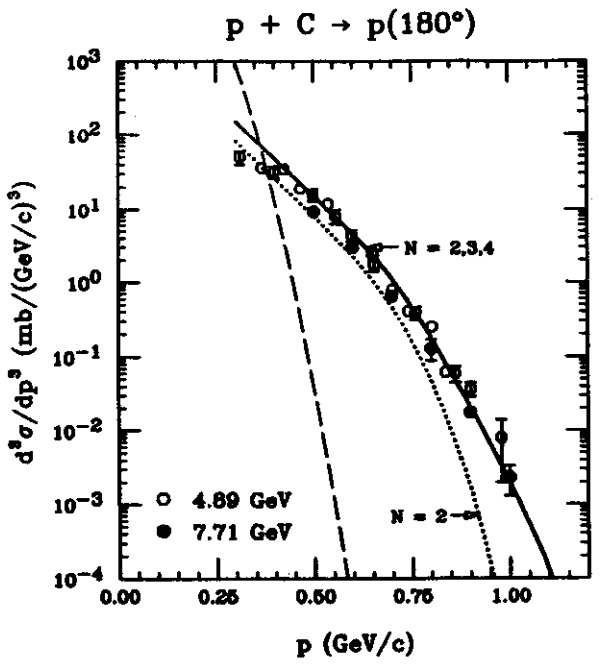

Fig. 1. Cross section for backward proton emission in proton-nucleus interactions. The data are from Refs. 4 (open circles) and 5 (filled circles). The solid line indicates the cross section for emission from the collisions with two, three, and four target nucleons. The dotted line indicates the contribution from collisions with two target nucleons (6). The long-dashed line represents a rough estimate for the maximum contribution to the cross section from the fragmentation process, given by $Z\sigma_R f(p)$ with the reaction cross-section σ_R = 255 mb.

Figure 1 shows the spectrum of the backward emitted protons in high-energy proton-carbon collisions.[4,5] The Fermi momentum limits the low-momentum region where protons originate from the decay of residual nucleus. Further, the Fermi momentum represents the edge of the phase space for the direct emission in an interaction with a single target nucleon. The tails in the spectra, that saturate with the bombarding energy and extend into extreme momenta are also observed in the backward direction in the spectra of mesons, as well as when heavier nuclei, mesons, and leptons are used as projectiles.

The threshold energy for antiproton production in pp collisions is equal to 5.6 GeV. The production of antiprotons was first observed[6] in p-copper collisions at energies 5 and 6.1 GeV. Later the observations have been extended[7] down to 2.9 GeV. (No observations of production in pp collisions were reported up to now for energies below 11 GeV.) The Fermi motion can be used to explain the production cross-sections, assuming an interaction of projectile proton with single target nucleon, but only for energies close to the threshold, Fig. 2.

The dynamics can be studied by examining the products of the reaction or the fate of a projectile. The weakness of electromagnetic interaction ensures that an electron scattered quasielastically from a nucleus interacts only once. The cross section can be factorized for high energies into a factor associated with electromagnetic interaction, and a function F(y) related to the distribution of nucleons in energy and momentum S(p,E) with

$$F(y) = 2\pi \int^{\bar{E}} dE \int_{|y+E-\bar{E}|}^{\infty} dp\, pS(p,E). \qquad (1)$$

Here $y = -q + \sqrt{(\bar{E}+\omega)^2 - m^2}$, and q and ω are the momentum and energy, respectively, transferred to the nucleus, $\bar{E} = m - \Delta$, and Δ is the

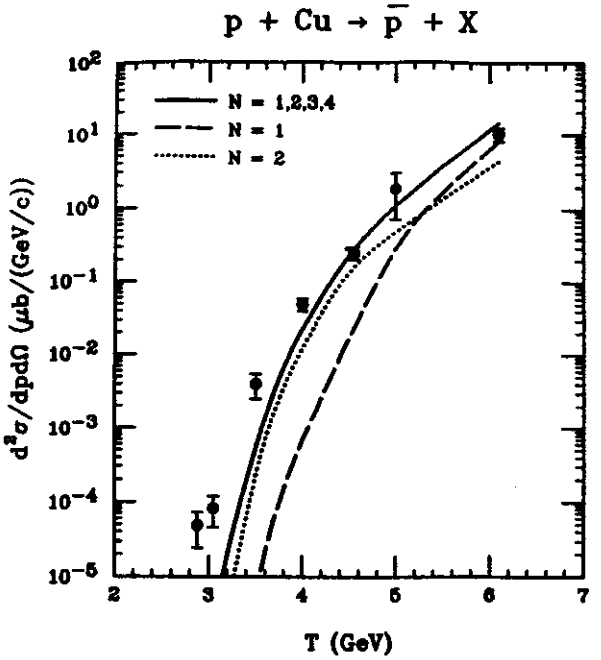

Fig. 2. Cross section for antiproton production as a function of bombarding energy for protons incident on copper. The normalized data are from Refs. 6 and 7. The solid line indicates the calculated cross section for production in collisions with 1, 2, 3, and 4 target nucleons. The long-dashed and dotted lines indicate, respectively, the contributions from collisions with one and two nucleons.

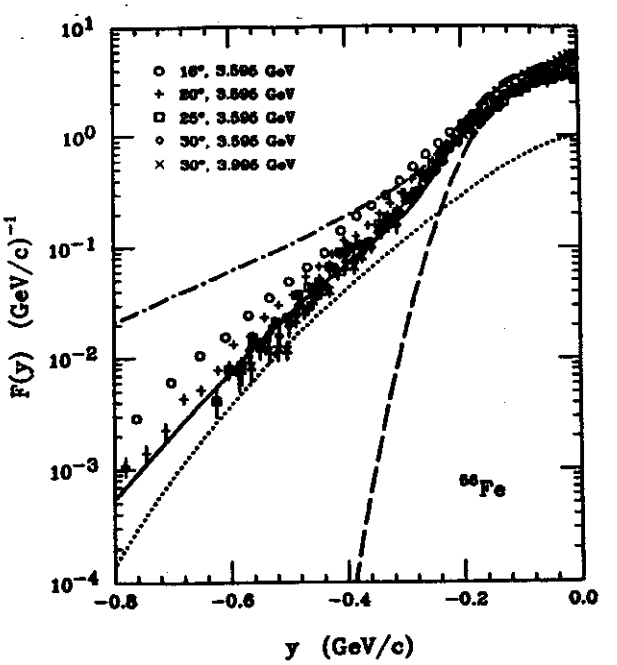

Fig. 3. Scaling function for ^{56}Fe. The experimental data is from Ref. 2. The solid line indicates the result obtained from the relation of the scaling function to the spectral function. Dashed and dotted lines indicate, respectively, contributions from one and two interacting nucleons in the spectral function. The dash-dotted line indicates the result that follows when one simplifies the energy dependence of the spectral function making the scaling function a functional of momentum distribution only.

separation energy. In Fig. 3 the scaling function F(y) extracted from the data[2] is compared with the function evaluated assuming an independent-particle motion in the mean potential field

$$S(p,E) = f(p)\delta(E - (m - B)), \qquad (2)$$

with f - the nucleon momentum distribution taken from the oscillator model, and B - the binding energy per nucleon. The experimental function F(y) exhibits a tail extending to large negative values of y, that cannot be explained by considering only independent motion of nucleons.

Within the real-time many-body theory we examined the possibility of going beyond the superposition of binary collisions in describing a high-energy reaction process. The evolution of the distribution of particles g(p,x) is governed by the equation of Boltzmann form, written here for fermions,

$$\frac{\partial g}{\partial t} + \mathbf{v}\cdot\frac{\partial g}{\partial \mathbf{r}} + \mathbf{K}\cdot\frac{\partial g}{\partial \mathbf{p}} = \Sigma^{<}(1 - g) - \Sigma^{>}g\ . \qquad (3)$$

The vector K is the average force and $\Sigma^{<}$ and $\Sigma^{>}$ are the production and absorption rates, respectively. We found[8] that the rates can be expanded in the number of interacting particles,

$$\Sigma^{<} = \Sigma_2^{<} + \Sigma_3^{<} + \ldots\ , \qquad (4)$$

where $\Sigma_k^{<}$ is a rate for production in the processes involving k particles in the initial state. These rates assume a simple form

$$\begin{aligned}\Sigma_k^{<}(p,E) &= \sum_n \int dp_1' \ldots dp_k' dp_1 \ldots dp_{n-1}\delta(p_1' + \ldots + p_k' - p \\ &\quad - p_1 - \ldots - p_{n-1})\delta(E_1' + \ldots + E_k' - E \\ &\quad - E_1 - \ldots - E_{n-1})g(p_1')\ldots g(p_k')(1 - g(p_1)) \\ &\quad \times \ldots(1 - g(p_{n-1}))|T^{k\to n}|^2\ , \qquad (5)\end{aligned}$$

where $T^{k\to n}$ is an amplitude for a process with k particles in the initial state and n in the final. The many-body amplitudes can be expanded in terms of the amplitudes with two bodies in an initial state (that are treated as elementary) and the propagators.

Numerically we have found that the process indicated in Fig. 4 with two target nucleons, gives a large contribution to the backward proton production. On using $g(p,x) = f(p)\rho(x)$,

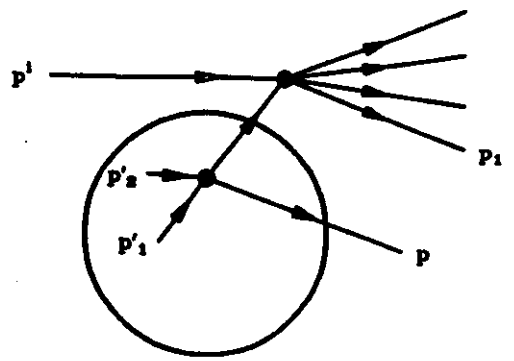

Fig. 4 Three-body collision process.

where ρ is spatial density, and integrating the production rate over the projectile trajectory, we get for the production cross section in the limit $p^i \to \infty$:

$$\frac{d^3\sigma}{dp^3} = \frac{1}{(2\pi)^3 E} Z\sigma_{NN} \bar{\rho}\int dp_1' dp_2' f(p_1') f(p_2') \frac{1}{2}|T|^2 \times \left(\frac{2m}{(p_1' + p_2' - p)^2 - m^2}\right)^2 (2(m - B) - p_1'^z - p_2'^z - E + p^z)\theta(2(m - B) - p_1'^z - p_2'^z - E + p^z) . \quad (6)$$

The probability of two nucleons encountering each other is proportional to the average density in a nucleus $\bar{\rho} = \frac{1}{A}\int d^3x\ \rho^2(x)$. In addition to the production in interactions of projectile with two target nucleons, one expects the production in interactions with three and more target nucleons. The respective partial cross sections are proportional to the higher powers of density. The net estimated cross section from the tree processes such as in Fig. 4, representing an expansion of the target wave function, is shown in Fig. 1. The dependence on density results in the nontrivial dependence of the cross section for backward emission on target mass[3], going beyond the proportionality to proton number, in fair agreement with data.

When the same processes as in the backward proton emission are included in the antiproton production, in addition to the process with a single target nucleon, and with the production taking place in the interaction vertex involving a projectile, much improved agreement with the subthreshold data is obtained, Fig. 2. The cross section is normalized by assuming that an antiproton can be produced only in the first collision of the projectile.

Finally, we take into account the multiparticle processes in the electron scattering by calculating the scaling function F from Eq. (1), on approximating S(p,E) in a consistent manner by

$$f(p)\delta(E - (m - B)) + \left(\frac{2m}{E^2 - p^2 - m^2}\right)^2 \left[\bar{\rho}\int dp_1' dp_2' \times f(p_1')f(p_2')\frac{m}{(2\pi)^3 E_{\mathbf{p}_1'+\mathbf{p}_2'-\mathbf{p}}}\frac{1}{2}|T|^2 \times \delta(E + E_{\mathbf{p}_1'+\mathbf{p}_2'-\mathbf{p}} - 2(m - B)) + \ldots\right], \quad (7)$$

The dots in (7) indicate the terms involving 3 and 4 target nucleons. The result for F(y) is shown in Fig. 3.

Current efforts concentrate on the use of the NN scattering matrix extracted from microscopic calculations, rather than parameterized, and on the description of backward pion production.

References

1. S. Frederiksson et al., Phys. Rep. 144, 187 (1987).

2. D. B. Day et al., Phys. Rev. Lett. 59, 427 (1987); R. D. McKeown, AIP Conference Proc. 176, 490 (1988).
3. P. Danielewicz, report MSUCL-709, 1989.
4. J. V. Geaga et al., Phys. Rev. Lett. 45, 1993 (1980).
5. A. M. Baldin et al., report JINR P1-11302, 1978.
6. O. Chamberlain et al., Phys. Rev. 100, 947 (1955).
7. D. E. Dorfan et al., Phys. Rev. Lett. 14, 995 (1965); A. Shor et al., report LBL-17067, 1984.
8. P. Danielewicz, Ann. Phys. (N.Y.) 197, 154 (1990).

CUTTING RULES IN MANY-BODY THEORY

P. Danielewicz

The method of real-time Green's functions[1,2] permits one to address the properties of a many-body system in a ground state, in a finite temperature equilibrium state, and in a nonequilibrium situation, in a consistent manner. This is in contrast to the imaginary-time method that exploits specific properties of an equilibrium state, and with the method of chronological Green's functions that is suited for the ground-state problems. The real-time Green's functions are, in particular, commonly used to derive transport equations valid in the quasiparticle limit.

The applicability of the real-time method has been hindered by the complexity of the theory when going beyond the lowest-order approximations to quantities of interest, like particle densities and particle production and absorption rates. It has not been possible to ensure the positive definiteness of such quantities and, further, to identify the physical processes accounted for within a given approximation.

We examine[3] the high-order structure of diagrammatic expansion in the real-time many-body theory. We demonstrate the existence of cutting rules for diagrams that may e.g. represent the production and absorption rates in the medium. The rules allow to disentangle the amplitudes and densities in a medium. For an expectation value of a product of operators A, B,..., $M^\dagger$, we find

$$\begin{aligned}&\langle A(x_1)B(x_2)\ldots M^\dagger(x_k)\rangle \\ &= \sum \frac{1}{S}\int dx_1^1\ldots\int dx_1^r\ldots a(x_1;x_1^1,\ldots)b(x_2;x_1^2,\ldots)\ldots \\ &\quad\times m^*(x_k;x_1^n,\ldots)G^>(x_1^1,x_1^2)\ldots G^<(x_2^2,x_2^1) \\ &\quad\times\ldots G^>(x_1^k,\ldots)\ . \qquad (1)\end{aligned}$$

Here a, b,..., m^*, are the dressed retarded amplitudes for the operators. The functions

$$G^<(x_1,x_2) = \langle\psi^\dagger(x_2)\psi(x_1)\rangle \qquad (2)$$

and

$$G^>(x_1,x_2) = \langle\psi(x_1)\psi^\dagger(x_2)\rangle, \qquad (3)$$

represent single-particle densities.

The particle production and absorption rates can be written in terms of the expectation values of products of two operators[4] that can be expanded in the manner indicated in Eq. (1). Physically this corresponds to the expansion in the number of interacting particles. The results for the rates[3] extend the S-matrix theory to the situation where more than two bodies collide and also when the bodies are medium excitations.

As an example of the application of general results, a resummation has been carried over repeated interactions of particles and holes for the single-particle production and absorption rates. Further, the formulae for the absorption and production rates of collective excitations have been derived.

The results can be further used in transport theory of nuclear collisions in treating the subthreshold production,[5] involving several nucleons, the absorption involving several particles, and the light fragment production. Appropriate relativistic modifications in the theory can be found in Ref. 6. Current efforts concentrate on deuteron production.

References

1. L. P. Kadanoff and G. Baym, Quantum Statistical Mechanics, Benjamin, New York, 1962.

2. B. Bezzerides and D. F. DuBois, Ann. Phys. (N.Y.) 70,10(1972).
3. P. Danielewicz, Ann. Phys. (N.Y.) 197,154 (1990).
4. P. Danielewicz, Ann. Phys. (N.Y.) 152,239 (1984).
5. P. Danielewicz, report MSUCL-709, 1989.
6. St. Mrowczynski and P. Danielewicz, U. of Regensburg report TPR-89-34, accepted for publication in Nuclear Physics B.

GREEN FUNCTION APPROACH TO TRANSPORT THEORY OF SCALAR FIELDS

St. Mrowczynski[a] and P. Danielewicz

It is common to describe the collisions of heavy nuclei at intermediate energies using the Boltzmann equation. We analyze the derivation of relativistic transport equations of possible importance for the relativistic collisions, from quantum field theory. We begin with[1] two simple models of scalar fields with the interaction terms in the lagrangians proportional, respectively, to ϕ^3 and $(\phi\phi^*)^2$, in order to elucidate the peculiarities of the problem. Using other methods, and in different context, the transport theory of scalar fields has been studied by Carruthers and Zachariasen[2] and by Cooper and Feigenbaum[3].

We start by defining a Green function Δ on a contour in time. The contour starts in the remote past, and the Green function Δ reduces to the more standard functions $\Delta^{>(<)}$, $\Delta^{\pm}$, for the specific ranges of arguments on the contour. The equation of motion for the Green function Δ is of the Dyson-Schwinger form. From the respective equations of motion for the functions $\Delta^{>(<)}$, the mass shell and transport equations for particles and antiparticles can be obtained in the quasiparticle limit. The self-energies from the equations of motion coincide with the production and absorption rates in that limit. The pairing approximation and perturbation expansion for the self-energies is discussed. The analysis appears simpler in the $(\phi\phi^*)^2$ than in the ϕ^3 model. This is because the internal structure of self-energies is more complicated in the lowest nontrivial order in the latter model. The structure of self-energies is reflected in the scattering amplitudes in the quasiparticle limit.

Current efforts concentrate on the derivation of the equations for a system with fermions and vector particles.

a. Institut für Theoretische Physik, Universität Regensburg, Postfach 397, 8400 Regensburg, West Germany, and Institute for Nuclear Studies, ul. Hoza 69, 00-681 Warsaw, Poland

References

1. St. Mrowczynski and P. Danielewicz, Nuclear Physics B in print.
2. P. Carruthers and F. Zachariasen, Phys. Rev. D13,950(1976).
3. F. Cooper and M. Feigenbaum, Phys. Rev. D14, 583(1976).

EIKONAL MODELS OF FRAGMENTATION

G. Bertsch, H. Esbensen[a], A. Sustich

Reaction cross sections at high energy have shown to be very useful to get structural information about nearly unbound nuclei.[1] We have therefore begun to reexamine the theory of these reaction cross sections. Here we compare three models of nuclear fragmentation based on an eikonal approximation.

We are interested in the fragmentation of a projectile interacting with some target. We consider the projectile wave function in some detail but only consider the target as a density distribution. Two of the models are based on the eikonal phase a nucleon of the projectile acquires in going past the target. For protons, this is taken as

$$\chi_p(b) = \frac{i}{2}\int_{-\infty}^{\infty}[\sigma_{pp}\,\rho_{T_p}(\sqrt{z^2+b^2}) + \sigma_{np}\rho_{T_n}(\sqrt{z^2+b^2})]dz$$

where ρ_{T_p} (ρ_{T_n}) is the target proton(neutron) density. At a projectile energy of 800MeV/A, we use $\sigma_{nn}=\sigma_{pp}=47$mb and $\sigma_{np}=38.5$mb.

The wave function of a projectile nucleon, ψ_α, is modified by the scattering according to

$$\psi(\vec{s},z) = e^{i\chi(\vec{b}+\vec{s})}\psi_\alpha(\vec{s},z)$$

where $\vec{b}$ is the impact parameter with respect to the target. The probability that this nucleon remains in its initial state is given by

$$P_\alpha(b) = |\langle\psi_\alpha|e^{i\chi(\vec{b}+\vec{s})}|\psi_\alpha\rangle|^2$$

The probability that the entire projectile remains in its ground state is then a product ofthe probabilities that all nucleons remain in their initial configuration,

$$P_0(b) = \prod_{\tau\ell j}(P_{\tau\ell j})^{n_{\tau\ell j}}\ .$$

The product is over all occupied nucleon shells with occupation number $n_{\tau\ell j}$. The reaction cross section is given by

$$\sigma_R = \int_0^\infty 2\pi b db(1 - P_0(b)).$$

This is our "diffractive eikonal" model. The reaction probability includes both the possibility of the absorption of a nucleon as well as its diffraction into a state different from its initial state.

The diffraction of a nucleon into a different state will leave the projectile in an excited state. Neutron drip line nuclei have very low neutron separation energies, and hence, the excited states are all (or mostly) unbound. In this case, the above model should give a reasonable estimate of the reaction cross section. However, for tightly bound nuclei, the low energy excited states are bound, and diffraction into these states will leave the projectile intact. Thus, the survival probability for a nucleon is given by

$$P_\alpha(b) = \sum_{n,\text{bound}}|\langle\psi_n|e^{i\chi(\vec{b}+\vec{s})}|\psi_\alpha\rangle|^2\ .$$

If we consider the extreme case where all projectile states are bound, closure over the states ψ_n yields the abrasion model[2] for the probability,

$$P_\alpha^{abr}(b) = \langle\psi_\alpha|e^{-2\mathrm{Im}\chi(\vec{b}+\vec{s})}|\psi_\alpha\rangle\ .$$

A third model is based on absorption by a nucleus-nucleus optical potential.[3] Similar to the abrasion model, the projectile nucleus survival probability is

$$P_0^{AAO}(b) = e^{-2Im\chi(b)} .$$

Here the nucleus-nucleus eikonal phase is $\chi(b) = \chi_{pp} + \chi_{pn} + \chi_{np} + \chi_{nn}$, where we have defined

$$\chi_{np}(b) = \frac{i}{2}\sigma_{np}\int d^2s\, \tilde{\rho}_{P_p}(s)\,\tilde{\rho}_{T_n}(\vec{b}+\vec{s})$$

and

$$\tilde{\rho}(s) = \int_{-\infty}^{\infty} dz\, \rho(\vec{s},z) .$$

We also use the models to study the removal of one or two loosely bound valence neutrons from a tightly bound core. We assume any excitation of the valence neutron(s) results in the desired breakup, whereas any core excitation will produce further disintegration of the projectile. The probability for removal of the valence neutron(s) is thus,

$$P_{frag}(b) = (1 - P_{val}(b))P_{core}(b)$$

where P_{val} (P_{core}) is the product of probabilities for all valence(core) occupied states. For the nucleus-nucleus optical model, the valence(core) density of the projectile is used to calculate a separate eikonal phase for the valence(core).

Figure 1 shows the results of the three models for a calculation of the total reaction and two neutron removal cross sections for ^{11}Li on varying size targets. All three models give similar results for the total cross sections. The two neutron removal cross sections show more variation, although all have a similar A_T dependence.

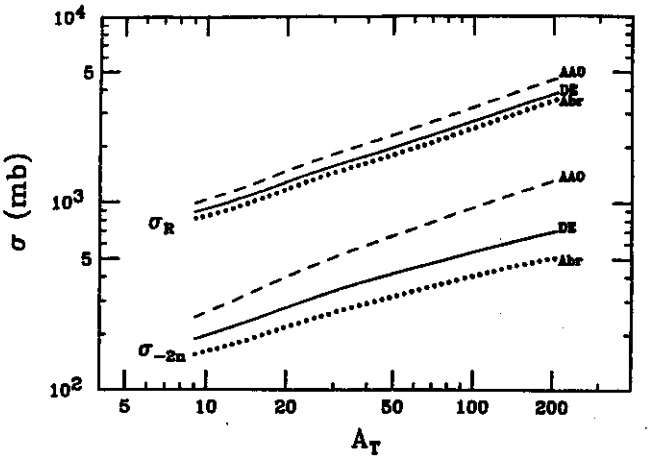

Fig. 1 The target mass dependence of the ^{11}Li reaction and two neutron removal cross sections for the three models, which are the abrasion model (Abr), the diffractive eikonal model (DE), and the nucleus-nucleus optical model (AAO).

Since the experimental two neutron removal cross section is a sum of both nuclear and coulomb contributions, the A_T (and hence, Z_T) dependence of the coulomb contribution is entirely dependent on how the nuclear contribution is subtracted out. The coulomb cross section, in turn, is related to the photoexcitation response of the projectile, and puts strong constraints on the dipole response, particularly at low excitations.[4] We believe that the diffractive eikonal model gives a better value for the nuclear (and hence,coulomb) contribution than previous estimates.[1]

---

a. Physics Division, Argonne National Laboratory, Argonne, IL

References

1. T. Kobayashi et al., Phys. Lett. 232B,51 (1989).
2. J. Hufner, K. Schafer, and B. Schurmann, Phys. Rev. C12,1888(1975).
3. G.F. Bertsch, B.A. Brown, and H. Sagawa, Phys. Rev. C39,1154(1989).
4. G.F. Bertsch and J. Foxwell, Phys. Rev. C41, 1300(1990).